Journal of
Manufacturing and Materials Processing

MDPI

Article

Energy-Based Characterization of Drilling-Induced Residual Stresses in AA7075-T6

Gorkem Tok [1,*], Ammar Tarık Dincer [1], Mustafa Bakkal [1] and Ali Taner Kuzu [2]

[1] Department of Mechanical Engineering, Istanbul Technical University, Istanbul 34437, Turkey; ammar.dincer@itu.edu.tr (A.T.D.); bakkalmu@itu.edu.tr (M.B.)
[2] Department of Mechanical Engineering, Isik University, Istanbul 34980, Turkey; alitaner.kuzu@isikun.edu.tr
* Correspondence: tokg15@itu.edu.tr; Tel.: +1-312-889-4937

Abstract

This study examines the influence of drilling parameters on thrust force, torque, active work, and axial residual stress formation in hot-forged and T6-treated AA7075, a critical high-strength aluminum alloy. A full factorial design was applied using three spindle speeds (800, 1000, 1200 rpm) and three feed rates (0.05, 0.10, 0.15 mm/rev). Cutting force and torque signals were measured using a dynamometer, and axial residual stresses were determined by X-ray diffraction at two locations along the hole depth, namely, the hole entrance (Point A) and the hole exit (Point B). The results show that feed rate is the dominant factor influencing drilling mechanics and residual stress formation, whereas spindle speed mainly affects the thermal and frictional conditions governing stress relaxation. A consistent asymmetry was observed between the two measurement locations, with the exit side exhibiting stronger stress relaxation behavior associated with breakthrough mechanics. Finally, the relationship between active work and axial residual stress is discussed using a qualitative, energy-based interpretation, highlighting active work as a physically meaningful indicator for drilling-induced residual stress evolution.

Keywords: hot forging; residual stress; 7075-T6; X-ray diffraction (XRD); drilling

1. Introduction

Residual stresses induced by machining operations significantly affect the dimensional accuracy, surface integrity, and fatigue life of structural components, particularly in high-strength precipitation-hardened aluminum alloys such as AA7075. Among various machining processes, drilling holds special importance, as holes often act as geometric stress concentrators and fatigue crack initiation sites. Consequently, controlling the residual stresses and surface quality generated during drilling is essential to ensure the long term reliability of aerospace and automotive components. AA7075, a member of the 7xxx series aluminum alloys, is widely utilized in aerospace structures owing to its high specific strength and relatively good machinability compared to steels. Its microstructure, primarily characterized by η ($MgZn_2$) precipitates, enables high mechanical strength but also increases sensitivity to thermal and mechanical loads during cutting [1,2]. Previous research has shown that machining-induced residual stresses strongly depend on cutting parameters such as cutting speed, feed rate, and tool geometry which govern the temperature distribution and plastic deformation beneath the surface [3].

In recent years, several studies have contributed to understanding residual stress mechanisms in aluminum alloys under various machining conditions. Denkena et al. [4]

Academic Editor: Steven Y. Liang

Received: 27 November 2025
Revised: 23 December 2025
Accepted: 27 December 2025
Published: 29 December 2025

reported that increasing cutting speed may promote a transition from tensile to compressive residual stresses due to reduced thermal gradients and improved chip evacuation. In drilling-specific investigations, Luo et al. [5] conducted an experimental and numerical study on the drilling of 7075-T6 aluminum alloy, demonstrating that feed rate is the dominant factor influencing axial force, torque, and temperature accumulation, while spindle speed primarily affects chip morphology and tool wear. Beyond drilling-focused studies, recent machining research has increasingly emphasized the role of process energy input and active work in governing thermal and residual stress evolution. Kara et al. [6] proposed a hybrid cutting model combining analytical force calculations with numerical thermal analysis, and highlighted that energy/active-work-based interpretations provide a physically meaningful route to connect mechanical power input with temperature distribution in cutting processes. In line with this perspective, Tok et al. [7] investigated residual stress and surface integrity in milling of hot-forged and T6-treated-AA7075 and reported strong relationships between cutting parameters and residual stress/roughness outcomes, providing a consistent framework for interpreting machining-induced stress formation in AA7075 systems.

Recent drilling studies have further emphasized the critical role of thermo-mechanical conditions on hole quality, tool performance, and subsurface integrity, particularly through temperature evolution and heat transfer mechanisms. Çakıroğlu and Acır [8] investigated the optimization of cutting parameters in drilling of Al 7075 alloys and demonstrated that feed rate is the most influential factor governing drill bit temperature, whereas cutting speed exhibits a secondary effect. Their findings confirmed that excessive thermal loading during drilling accelerates tool wear and alters near-surface material behavior, highlighting the importance of temperature control in drilling operations. Thermal phenomena become even more critical in deep-hole drilling processes, where heat dissipation is restricted due to the confined cutting zone. Biermann et al. [9] analyzed thermal aspects of deep-hole drilling of aluminum alloys using twist drills under minimum quantity lubrication (MQL) conditions and showed that increased feed rates significantly raise mechanical power and heat input into the workpiece. Their results indicated that heat accumulation within the hole adversely affects process stability and borehole quality, underscoring the dominant role of energy input in drilling-induced thermal behavior. To further quantify thermal loads during drilling, several researchers have proposed advanced heat transfer modeling approaches. Tai et al. [10] developed an inverse heat transfer method to determine heat fluxes on both the hole bottom and hole wall surfaces during deep-hole drilling. Their results revealed that frictional heat generation along the hole wall becomes increasingly significant with drilling depth, indicating that thermal effects persist well beyond the immediate cutting zone and continue to influence the subsurface material state. Beyond conventional drilling, process modifications such as vibration-assisted drilling have been explored to improve hole quality and mitigate damage mechanisms. Li et al. [11] proposed a mechanistic and experimental model for exit burr formation in vibration-assisted drilling of AA7075-T6, demonstrating that drilling forces, material deformation, and energy consumption strongly govern burr height and exit surface integrity. Their study highlighted that drilling-induced deformation and energy dissipation near the hole exit play a crucial role in determining local material response. Accurate measurement of temperature during drilling remains a major experimental challenge due to tool rotation and restricted access to the cutting zone. Le Coz et al. [12] developed an embedded thermocouple-based technique for measuring cutting tool temperature during drilling and milling under dry and MQL conditions. Their work demonstrated that elevated cutting temperatures significantly influence tool–workpiece interactions and may promote tensile residual stress formation in the near-surface region, especially under reduced lubrication conditions. More recently, the direct

relationship between thermal history and residual stress generation during drilling has been explicitly demonstrated. Chenegrin et al. [13] investigated the thermo-mechanical mechanisms governing residual stress formation during dry drilling and showed that localized overheating near the end of drilling induces intense plastic deformation, leading to high tensile residual stresses on the hole surface. Their findings confirmed that thermal history plays a decisive role in drilling-induced residual stress evolution, particularly in deep and confined drilling operations.

Complementary to drilling-focused investigations, turning operations have also been widely employed as a reference process to elucidate machining-induced residual stress mechanisms in high-strength aluminum alloys. Tok et al. [8] experimentally investigated residual stresses induced by turning of hot-forged and T6-treated-AA7075 using X-ray diffraction. Their results demonstrated that residual stress formation is governed by the combined effects of mechanical loading and thermal input, with tensile residual stresses becoming dominant when thermal effects prevail, while compressive stresses are associated with mechanically dominated cutting conditions. Furthermore, their study highlighted that cutting parameters primarily influence residual stresses through their effect on cutting power and active work, rather than geometric factors alone. These findings provide a strong energy-based framework for interpreting residual stress evolution and form a direct foundation for extending such analyses from continuous turning operations to drilling processes, where localized heat accumulation and cyclic tool engagement introduce additional complexity.

The combined effects of cyclic tool entry and exit, frictional heating, and localized strain concentration around the hole boundary create a complex residual stress field that differs from those observed in continuous machining processes such as turning. This knowledge gap limits the ability to accurately predict the evolution of drilling-induced residual stresses. Despite several contributions in machining, studies focusing specifically on drilling-induced residual stress in AA7075-T6 remain limited. First, existing studies mostly examine individual cutting parameters, while the combined effect of thermo-mechanical energy input active work and entrance–exit asymmetry has not been systematically investigated for AA7075-T6. Second, previous drilling research rarely compares residual stresses at both the hole entrance and exit, where breakthrough instability alters the local stress. Third, energy-based interpretations developed for turning or milling have not yet been extended to drilling of hot-forged aluminum alloys.

In contrast to existing drilling studies, the novelty of the present work lies in introducing an explicit energy-based interpretation of drilling-induced residual stress formation in hot-forged AA7075-T6. While previous studies have primarily focused on individual cutting parameters, temperature measurements, or surface integrity indicators, this study establishes a direct correlation between active work and axial residual stress evolution. Moreover, residual stresses are systematically evaluated at both the hole entrance and exit locations, capturing the effects of cyclic tool engagement and breakthrough-induced instability, which are rarely addressed simultaneously in literature. This approach extends energy-based frameworks previously developed for turning and milling to drilling operations, providing new mechanistic insight into thermo-mechanical stress generation in high-strength aluminum alloys. To address these gaps, the present study provides a systematic analysis linking active work to axial residual stress formation at two distinct drilling locations Point A and Point B in hot-forged and T6-treated AA7075. The results demonstrate a clear energy controlled thermo-mechanical mechanism governing drilling-induced residual stresses. Therefore, the present study aims to investigate the influence of drilling parameters on residual stress distribution and surface integrity in hot-forged AA7075-T6. This research serves as a direct continuation of the author's previous work on

turning of the same alloy [8], extending the understanding of machining-induced stress formation to the drilling process. Emphasis is placed on analyzing the correlation between calculated active work and the resulting residual stresses, providing mechanistic insight into how thermal mechanical energy input governs residual stress generation in multistage machining of high-strength aluminum alloys.

To clarify the structure and methodological workflow of the study, the overall technical route from drilling experiments to residual stress analysis and energy-based interpretation is summarized in Figure 1.

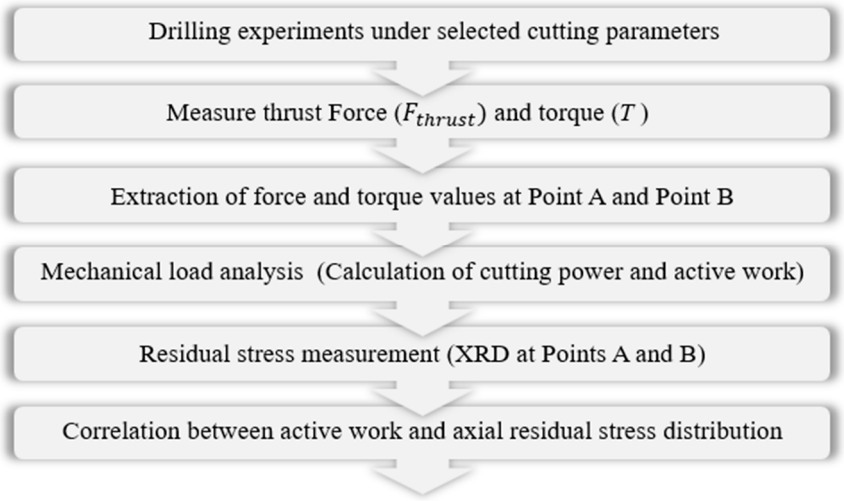

Figure 1. Flow chart of the present study illustrating the experimental procedure.

2. Materials and Methods

The material used for the workpieces in this study was AA7075-T6, a precipitation-hardened aluminum alloy commonly employed in aerospace and automotive applications due to its high strength-to-weight ratio. The chemical composition and mechanical properties of the material are presented in Tables 1 and 2, respectively. These values are consistent with those reported in the authors' previous investigation on turning of hot-forged and T6-heat-treated AA7075 alloy [8].

Table 1. Chemical compositions of the AA7075-T6 material [8].

Element	Si	Fe	Cu	Mn	Zn	Cr	Ti	Al
Content %	0.140	0.241	1.54	0.106	4.86	0.190	0.031	90.5

Table 2. Physical and mechanical properties of the AA7075-T6 material [8].

Ultimate Tensile Strength (MPa)	Yield Strength (MPa)	Elongation (%)	Young Modulus (GPa)	Hardness (HBW)	Thermal Conductivity, W/(m K)	Specific Heat Capacity, kJ/(kg K)
540	476	11	71.7	170	130	0.960

Each specimen was produced by hot forging followed by T6 heat treatment, ensuring homogeneous cooling conditions and consistent microstructural and mechanical properties across all samples. The mechanical tests and chemical composition analyses were conducted in accordance with EN ISO 6506-1 (Brinell hardness) [14], EN ISO 6892-1 (tensile testing) [15], and EN 573-3 (chemical characterization) [16] standards.

2.1. Experimental Methods

The machining experiments were conducted using vertical CNC machining center, specifically the VC-650 model (SPINNER, Sauerlach, Germany), with a maximum spindle speed of 8000 rpm. The experimental setup is illustrated in Figure 2. The workpiece is secured to a fixture (as illustrated in Figure 2) that is placed on top of a 9272 dynamometer (KISTLER, Winterthur, Switzerland) for measuring drilling forces and torque. The force and torque signals were amplified using a charge amplifier (Model 5070, Kistler, Winterthur, Switzerland) and subsequently recorded via a NI-9234 data acquisition board (National Instruments, Austin, TX, USA). Force and torque signals were recorded with a sampling frequency of 4650 Hz. For each drilling condition, cutting force and torque measurements were repeated twice under identical cutting parameters in order to evaluate measurement repeatability. The repeated measurements showed very close agreement, confirming stable drilling conditions. The selected drill bit (WIDIN, Changwon, Republic of Korea) for this study had a diameter (D) of 11.0 mm and was a solid carbide drill (P/N: 599064), with an overall length of 110 mm, a cutting length of 73 mm, and a shank diameter of 11 mm.

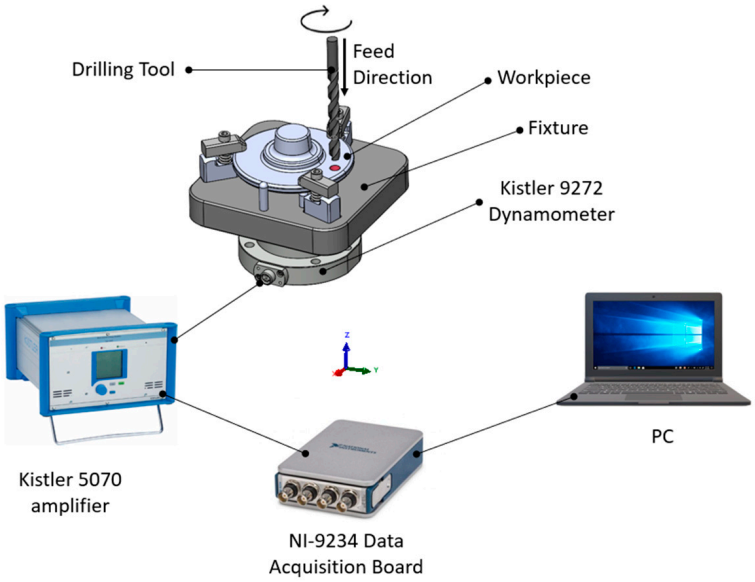

Figure 2. Schematic illustration of the experimental setup used for force and torque measurements.

In addition to the force–torque measurement setup shown in Figure 2, the complete drilling station and fixture arrangement used throughout the experiments are presented in Figure 3. This figure provides an overview of the CNC drilling machine and the clamping configuration, ensuring consistent rigidity and repeatability during all drilling trials. In drilling operations, the feed rate (f), expressed in mm/rev, is defined as the linear advance of the drill per spindle revolution, while the cutting speed (V_c), given in m/min, is determined from the rotational speed of the spindle (n) and the drill diameter (D), as described by Equation (1):

$$V_c = \pi D n \quad (1)$$

Here, f_r represents the feed per revolution (mm/rev), n is the spindle speed (rev/min) and all drilling operations were carried out under dry conditions. The experimental design followed a full factorial approach, enabling the comprehensive investigation of the effects of drilling parameters on residual stresses. The primary cutting parameters were spindle speed (n) at 800, 1000, and 1200 rev/min and feed rate (f) at 0.05, 0.10, and 0.15 mm/rev, and the resulting combinations used in the experiments are listed in Table 3 and cutting parameters were suggested and confirmed by the industrial partner. In order to ensure

consistent conditions, each test was performed with a new drill bit and identical clamping configuration. Following the drilling operations, the residual stresses were determined via X-ray diffraction (XRD) in accordance with the methodology detailed in Section 2.2. All measurements were performed in a controlled laboratory environment at 22 ± 1 °C to eliminate thermal variations.

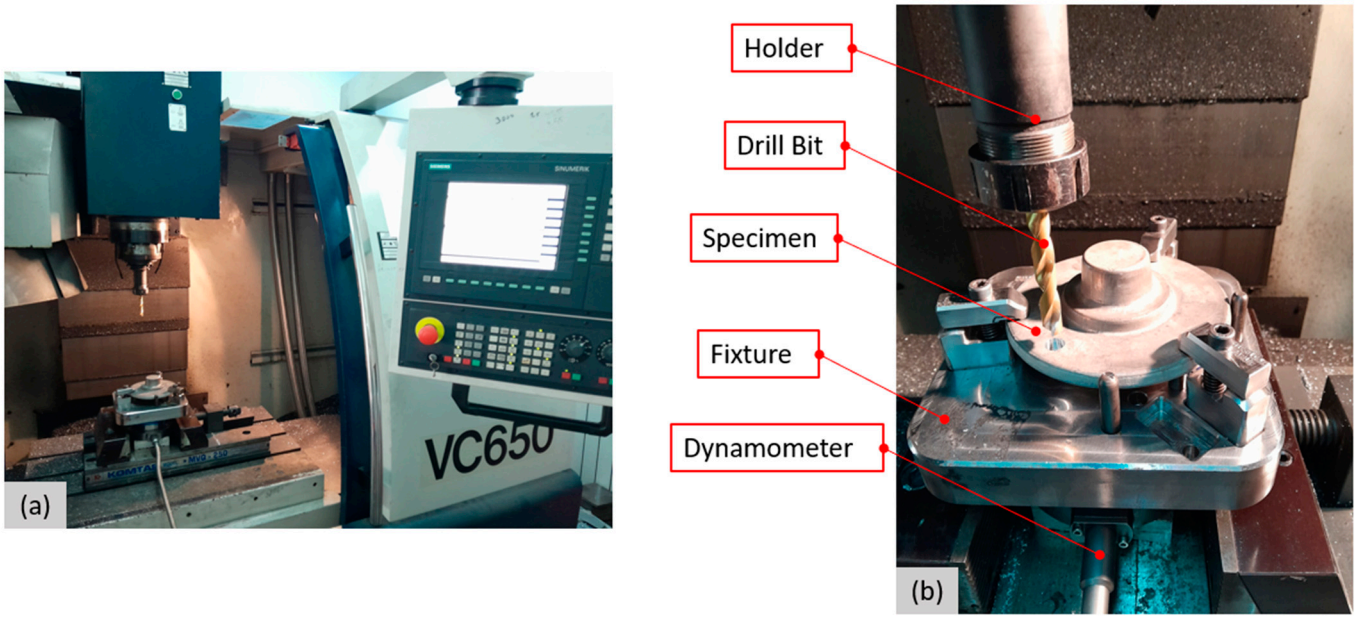

Figure 3. CNC drilling machine (**a**), experimental setup (**b**).

Table 3. Drilling parameter set used in the experiments. (# denotes the experiment number).

Experiment #	Spindle Speed (n) (rpm)	Feed Rate (f) (mm/rev)
1	800	0.05
2	1000	0.05
3	1200	0.05
4	800	0.10
5	1000	0.10
6	1200	0.10
7	800	0.15
8	1000	0.15
9	1200	0.15

2.2. X-Ray Diffraction Residual Stress Measurement Methodology

Residual stresses induced on the drilled hole surfaces were determined using the X-ray diffraction (XRD) technique in accordance with the EN 15305:2008 standard [17] employing an XStress 3000 G2R X-ray diffractometer (Stresstech, Jyväskylä, Finland). The XRD method is based on the principle that elastic deformation of crystal lattices alters the interplanar spacing, which consequently changes the diffraction angle according to Bragg's law ($n\lambda = 2d\ sin\theta$). By measuring the variation in the diffraction angle ($\Delta\theta$) as a function of the specimen tilt angle (ψ), the corresponding strain components can be calculated. The $\sin^2\psi$ method, widely accepted for residual stress evaluation, establishes a linear relationship between the interplanar strain (ε) and $\sin^2\psi$, where the slope of this line is directly related to the in-plane residual stress. This theoretical foundation allows for non-destructive quantification of near-surface stresses with high precision, making

XRD particularly suitable for evaluating machining-induced stress gradients [18]. The specifications of the X-ray diffractometer can be found in Table 4.

Table 4. X-ray diffraction parameter.

X-Ray Diffraction Parameter	Device Model	Radiation	Filter	2θ	Miller Indices [h k l]	Collimator Size
Specification/Values	XStress 3000 G2R	Cr–Kα	No Filter	156.7°	[2 2 2]	1 mm

To access the internal surfaces along the hole wall, each specimen was sectioned longitudinally through the hole center using Electrical Discharge Machining (EDM) as shown in Figure 4. This procedure was necessary to gain physical access to the measurement regions, as the internal wall of the drilled holes cannot be directly exposed for X-ray irradiation due to geometric constraints. EDM cutting also ensured minimal thermal or mechanical influence on the residual stress state, preserving the integrity of the measurement zones.

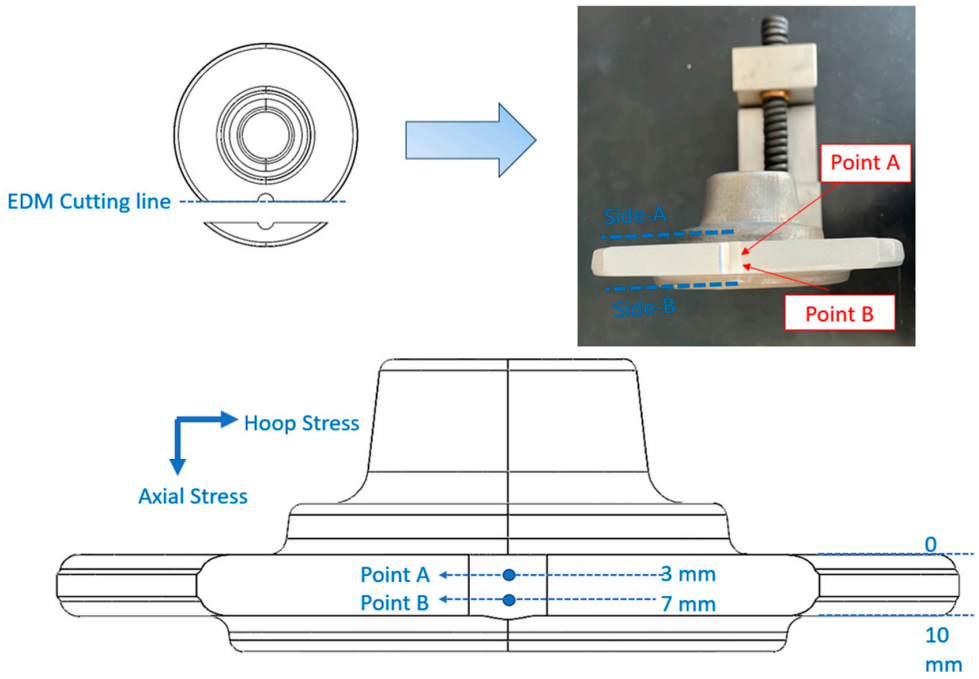

Figure 4. Representation of XRD measurement locations and stress orientations.

Residual stress measurements were performed at two distinct axial locations along the drilled hole wall to evaluate the stress distribution along the drilling direction. As illustrated in Figure 4, Point A corresponds to the region located 3 mm below the hole entrance while Point B was defined as the location positioned 3 mm from the hole exit surface, which corresponds to 7 mm from the upper (entry) surface of the 10 mm thick workpiece. This configuration allowed for evaluation of the stress distribution along the drilling direction and identification of possible asymmetry between the entry and exit sides. Each measurement was taken in two perpendicular directions (Hoop and Axial) to account for potential anisotropy in the stress field caused by the cyclic nature of tool engagement and withdrawal.

The data were analyzed using the $\sin^2\psi$ method, assuming biaxial stress conditions parallel to the hole surface. The elastic modulus (E = 72 GPa) and Poisson's ratio (ν = 0.33) were adopted from standard mechanical properties of AA7075-T6.

2.3. Mechanical Load Analysis

During drilling, the tool–workpiece interaction generates complex mechanical and thermal loads that directly influence tool wear, chip formation, and residual stress development on the machined surface. A precise evaluation of the mechanical load is therefore essential for quantifying the energy input process and understanding its correlation with the resulting residual stress field. In this study, the cutting power (P_c), which represents the mechanical energy transferred from the spindle to the cutting zone per unit time, was calculated from the experimentally measured instantaneous drilling torque (T) and the spindle speed (n) according to Equation (2):

$$P_c = \frac{2\pi T n}{60} \quad (2)$$

where T is expressed in N·m and n in revolutions per minute (rev/min). The calculated power quantifies the total mechanical effort exerted by the tool during chip removal, reflecting the coupling of frictional and plastic deformation energy. This approach aligns with methods used in previous studies on drilling and energy-based modelling of aluminum alloys [9]. The machining time (t_m) for each hole was obtained from the ratio between the drilled depth (L) and the feed rate (f) as follows:

$$t_m = \frac{L}{f \cdot n} \quad (3)$$

The active work (W_a) which represents the total mechanical energy input during drilling, was then derived by integrating the cutting power over the machining time according to Equation (4):

$$W_a = P_c \cdot t_m \quad (4)$$

The active work quantifies the accumulated mechanical energy acting on the cutting zone and is closely associated with heat generation and plastic strain energy within the near-surface layer. As pointed out by Biermann et al. [9], a significant portion of the mechanical energy introduced during drilling is dissipated as heat at the tool–chip and tool–workpiece interfaces, thereby influencing the magnitude and distribution of residual stresses.

Complementary studies have further demonstrated that mechanical energy input plays a decisive role in subsurface stress evolution. Kwong et al. [19] showed that increased cutting energy intensifies plastic deformation beneath the machined surface, leading to pronounced residual stress gradients in aluminum alloys. Similarly, Tai [20] reported that torque-based energy input provides a reliable basis for quantifying thermal loading in drilling processes, particularly in cases where direct temperature measurement is challenging. More recent investigations on drilling of aluminum alloys have also confirmed that drilling power and energy dissipation strongly govern surface and subsurface integrity, including residual stress development [21].

In the present study, the calculated values of W_a were therefore used as a key indicator to evaluate the correlation between mechanical energy input and residual stress generation in the hot-forged and T6-heat-treated AA7075 alloy. This analysis provides a fundamental basis for interpreting how process parameters govern the energy balance and surface integrity during high-performance drilling of aluminum components.

3. Results

3.1. Effect of Cutting Parameters on Force and Torque

The thrust force and torque signals were recorded throughout each drilling operation. Based on the measurement locations defined in Section 2.2, the thrust force and torque values corresponding to Points A and B were extracted from the time-domain signals shown in Figure 5. These locations were used to evaluate the variation of cutting forces along the drilling depth by extracting the maximum force and torque values, as illustrated

in Figure 6. The thrust force and torque were measured simultaneously during drilling to characterize the mechanical loading on the drill and workpiece. For each measurement point, the force and torque values were determined at the instant when the conical tip of the drill completely passed the corresponding depth. Since the drill tip has an included angle of 140° and diameter of the tool is 11 mm, the cone height was calculated geometrically as 3.16 mm. Accordingly, the total vertical travel of the drill corresponding to full penetration of Points A and B was 6.16 mm and 10.16 mm, respectively. Using the relationship between distance, feed rate, and time, the penetration distances were converted into corresponding time intervals according to Equations (5) and (6):

$$S = v_f t \tag{5}$$

$$v_f = \frac{f \times n}{60} \tag{6}$$

where s is the drilling depth (mm), v_f is the feed velocity (mm/s), f is the feed per revolution (mm/rev), and n is the spindle speed (rpm).

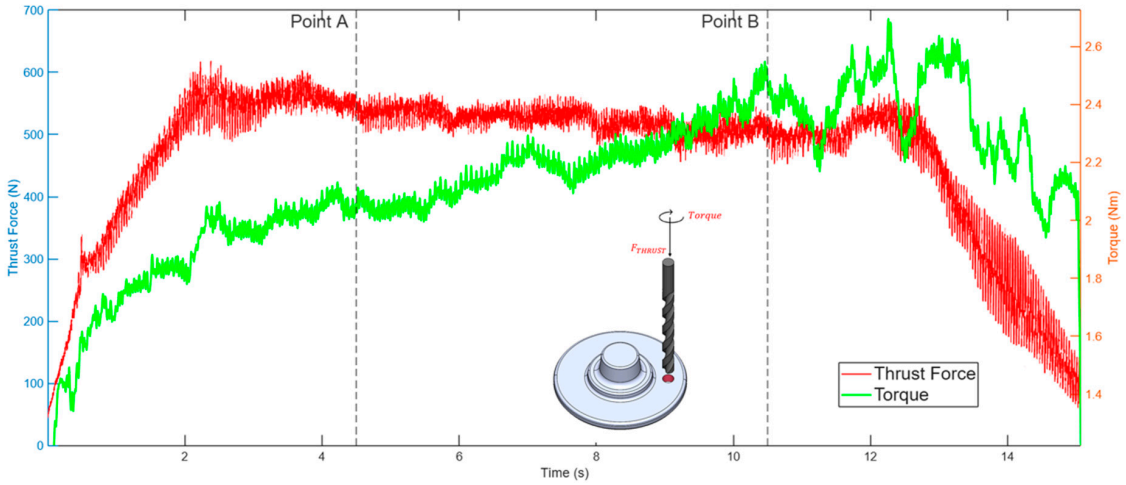

Figure 5. Exp #1 thrust force and torque measurement. (The vertical dashed lines indicate the measurement locations corresponding to Point A and Point B).

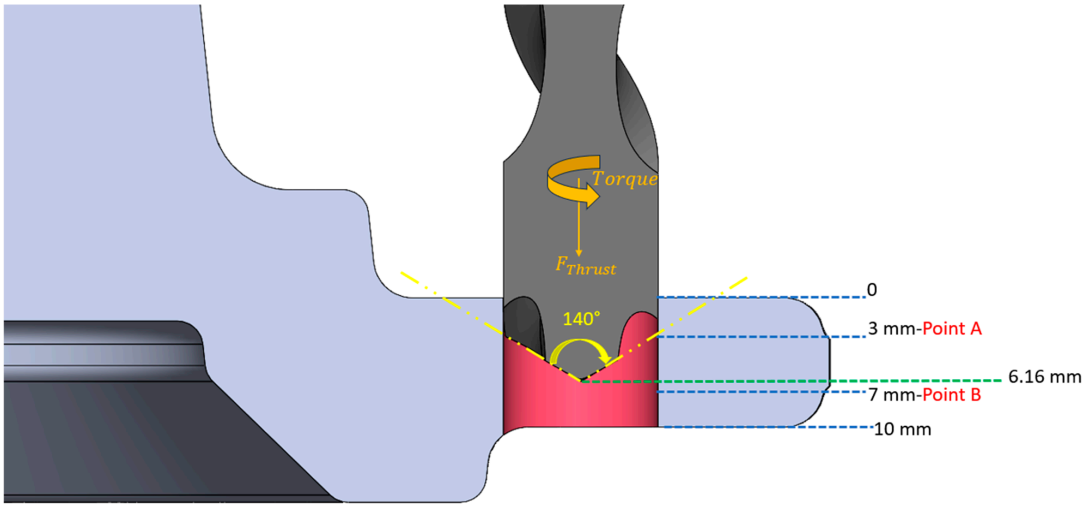

Figure 6. Schematic representation of drilling geometry showing the measurement of Point A where thrust force, torque and residual stress values were measured. (The red region represents the cutting engagement zone, the gray area denotes the drill body, and the blue region indicates the workpiece; dashed lines mark the measurement locations Points A and B).

The force and torque signals corresponding to these calculated time intervals (t_A and t_B) were then extracted from the recorded time series to determine the instantaneous cutting loads at both reference points. To improve clarity in the interpretation of the results, the drilling condition corresponding to the lowest thrust force value (Experiment No. 3) was selected as a reference condition and thrust force and torque values obtained under the remaining drilling conditions were therefore expressed as relative variations (ΔF and ΔT) with respect to this reference case.

The drilling experiments demonstrated that both thrust force and torque are strongly influenced by the feed per revolution, whereas spindle speed primarily affects the thermo-mechanical conditions in the cutting zone. The measured results for Point A and Point B are summarized in Tables 5 and 6, respectively. An overall comparison shows that an increase in feed from 0.05 mm/rev to 0.15 mm/rev caused a consistent rise in both thrust force and torque, reflecting the increase in uncut chip thickness and the enlargement of the shear deformation zone. This behavior is in good agreement with the experimental drilling study reported by Parasuraman et al. [22], who demonstrated that thrust force and torque in aluminum-based materials strongly scale with chip-load-dependent plastic deformation and feed rate.

Table 5. Thrust force, residual stress and standard deviation, power and active work measurement for Point A. (# denotes the experiment number).

Measurements of Point A											
Exp No. #	**Spindle Speed (*n*)**	**Feed Rate (mm/rev)**	**ΔF_{THRUST} (N)**	**ΔTorque (Nm)**	**t_x (s)**	**Hoop Stress (MPa)**	**STD ± [MPa]**	**Axial Stress (MPa)**	**STD ± [MPa]**	**Power (W)**	**Active Work (J)**
1	800	0.05	56.77	0.13	4.50	−253.1	18.6	−212.0	26.3	10.54	158.1
2	1000	0.05	139.15	0.44	3.60	−134.9	38.7	−135.9	21.5	46.45	557.4
3	1200	0.05	0.00	0.00	3.00	−238.9	12.6	−233.2	22.8	0.00	0.00
4	800	0.10	176.50	1.22	2.25	−195.4	30.8	−205.3	19.3	102.56	769.2
5	1000	0.10	160.99	1.38	1.80	−165.2	30.3	−219.1	24.3	144.75	868.5
6	1200	0.10	105.76	0.69	1.50	−210.6	55.0	−223.4	37.3	86.28	431.4
7	800	0.15	347.53	2.48	1.50	−216.5	24.9	−181.7	11.6	207.95	1039.8
8	1000	0.15	319.03	2.56	1.20	−106.7	19.7	−181.3	22.0	267.60	1070.4
9	1200	0.15	263.11	1.57	1.00	−333.8	15.7	−188.9	15.6	197.39	658.0

Table 6. Thrust Force, residual stress and standard deviation, power and active work measurement for Point B. (# denotes the experiment number).

Measurements of Point B											
Exp No. #	**Spindle Speed (*n*)**	**Feed Rate (mm/rev)**	**ΔF_{THRUST} (N)**	**ΔTorque (Nm)**	**t_x (s)**	**Hoop Stress (MPa)**	**STD ± [MPa]**	**Axial Stress (MPa)**	**STD ± [MPa]**	**Power (W)**	**Active Work (J)**
1	800	0.05	44.26	0.62	10.50	−311.3	31.6	−247.5	76.5	51.94	779.1
2	1000	0.05	123.82	0.57	8.40	−78.8	48.8	−106.1	42.6	59.52	714.2
3	1200	0.05	0.00	0.00	7.00	−143.8	14.2	−202.1	8.9	0.00	0.00
4	800	0.10	178.45	1.56	5.25	−206.8	11.2	−212.7	20.3	130.71	980.4
5	1000	0.10	104.98	2.08	4.20	−256.8	36.1	−171.5	27.5	217.83	1307.0
6	1200	0.10	64.29	0.90	3.50	−230.0	28.6	−238.1	23.7	112.84	564.2
7	800	0.15	295.26	2.66	3.50	−172.0	14.5	−139.5	19.4	222.65	1113.2
8	1000	0.15	235.99	2.77	2.80	−53.7	18.0	−127.1	16.3	290.28	1161.1
9	1200	0.15	209.13	1.46	2.33	−194.9	13.9	−170.6	14.6	183.12	610.4

On Point A, thrust force exhibited a clear increasing trend with feed rate. Lower thrust force values were obtained at the minimum feed level of 0.05 mm/rev, whereas a pronounced increase was observed as the feed was raised to 0.15 mm/rev. A similar

trend was identified for torque, which increased consistently with feed rate. These trends are associated with the increase in material removal rate, uncut chip thickness, and the corresponding resistance to chip extrusion during drilling.

At Point B, both thrust force and torque reached higher levels compared to Point A. This behavior is attributed to intensified frictional interaction, chip congestion, and secondary deformation effects occurring near the drill exit during the breakthrough stage. The higher mechanical loading at Point B confirms the asymmetric nature of drilling mechanics along the hole depth and highlights the critical influence of exit-side conditions on force and torque evolution.

This asymmetry is consistent with the observations reported by Gokce et al. [23], who showed that accumulated plastic deformation and secondary deformation effects near the hole exit lead to increased mechanical loading during drilling operations.

In contrast, spindle speed exhibited an inverse effect on both parameters. Increasing speed from 800 to 1200 rpm reduced average thrust force and torque across all feed levels. This reduction originates from thermally-induced material softening and a decrease in frictional resistance at elevated cutting temperatures. Recent investigations on drilling and hole-making processes have shown that higher spindle speeds promote more stable thermal conditions in the cutting zone and reduce frictional effects at the tool–chip interface, leading to lower mechanical loads during drilling [24]. Furthermore, it has been reported that increased spindle speed shortens the effective tool–workpiece contact duration and reduces the mechanical energy demand through improved heat dissipation [25]. The present results follow the same trend, indicating that spindle speed primarily controls the thermal field and lubrication state, while feed dictates the mechanical deformation component.

The statistical analysis of variance reinforces these trends. As summarized in Table 7a, the feed per revolution exhibited the highest influence on thrust force for Point A ($F = 44.99$, $p = 0.002$), while spindle speed had a weaker but still notable effect ($F = 5.87$). In Table 7b, feed remained the dominant factor ($F = 15.38$, $p = 0.013$), consistent with the increased sensitivity of the exit region to mechanical load. These findings are in good agreement with the drilling mechanics reported by Sikander et al. [26], who showed that thrust force and deformation-related mechanical loading increase significantly with feed rate due to the enlargement of the shear deformation zone and higher uncut chip thickness, while spindle speed primarily influences the thermo-mechanical conditions and chip evacuation behavior rather than the mechanical load itself.

For Point B, the ANOVA results summarized in Table 7d reveal an even stronger dependence of torque on feed per revolution ($F = 447.21$, $p = 0.000020$), with spindle speed also contributing significantly ($F = 89.31$, $p = 0.00048$). The substantially higher F-values observed at the exit side indicate intensified mechanical loading during the breakthrough stage. This behavior is consistent with the exit-side deformation and torque amplification mechanisms reported by Chao et al. [27], who demonstrated that chip congestion and secondary deformation during drilling lead to a pronounced increase in thrust force and torque, particularly near the hole exit region.

Figure 7a,b illustrate these combined effects: torque and thrust force both increase proportionally with feed but decrease at higher spindle speeds, with Point B consistently exhibiting higher absolute values. This pattern demonstrates the coupling between feed-driven mechanical deformation and speed-driven thermal relaxation.

Table 7. (**a**) Two-way ANOVA results for thrust force at Point A with feed per revolution (f) and spindle speed (n) as factors. (**b**) Two-way ANOVA results for thrust force at Point B with feed per revolution (f) and spindle speed (n) as factors. (**c**) Analysis of Variance (ANOVA) Table for Torque on Point A. (**d**) Analysis of Variance (ANOVA) Table for Torque on Point B.

(**a**)					
Source	**Analysis of Variance**				
	DF	**Adj SS**	**Adj MS**	**F Value**	***p* Value**
Feed Per Rev. (mm/rev)	2	92,907	46,454	44.99	0.002
n (rpm)	2	12,115	6057	5.87	0.065
Error	4	4130	1032	-	-
Total	8	109,152	-	-	-
(**b**)					
Source	**Analysis of Variance**				
	DF	**Adj SS**	**Adj MS**	**F Value**	***p* Value**
Feed Per Rev. (mm/rev)	2	57,108	28,554	15.38	0.013
n (rpm)	2	11,028	5514	2.97	0.162
Error	4	7424	1856	-	-
Total	8	75,560	-	-	-
(**c**)					
Source	**Analysis of Variance**				
	DF	**Adj SS**	**Adj MS**	**F Value**	***p* Value**
Feed Per Rev. (mm/rev)	2	6.1003	3.05015	75.75	0.000662
n (rpm)	2	0.8069	0.40345	10.02	0.02769
Error	4	0.1611	0.040275	-	-
Total	8	7.0683	3.493875	-	-
(**d**)					
Source	**Analysis of Variance**				
	DF	**Adj SS**	**Adj MS**	**F Value**	***p* Value**
Feed Per Rev. (mm/rev)	2	4.9143	2.45715	447.21	0.000020
n (rpm)	2	0.9814	0.49070	89.31	0.00048
Error	4	0.02198	0.005495	-	-
Total	8	5.91768	2.953345	-	-

Overall, the results confirm that feed per revolution is the dominant parameter controlling both thrust force and torque, whereas spindle speed regulates the thermal and frictional characteristics of the process. The Points A and B comparison, supported by ANOVA and the dynamic force–torque traces, clearly indicates that exit-side mechanics intensify tool loading due to restricted chip evacuation. These conclusions are in strong agreement with recent literature addressing the thermo-mechanical interactions governing drilling performance and surface integrity in high-strength aluminum alloys [26,27].

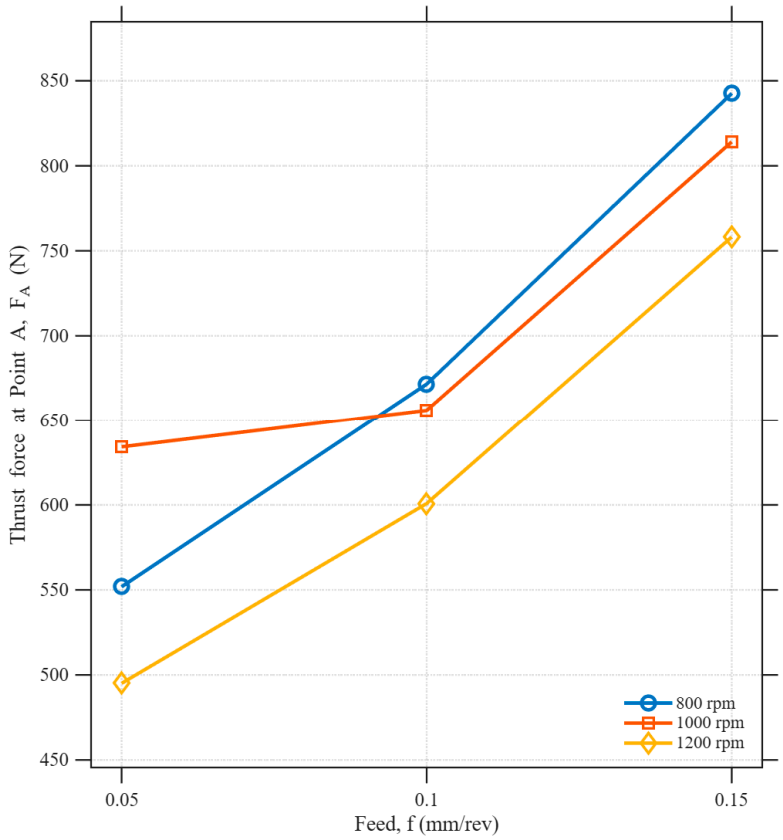

(**a**)

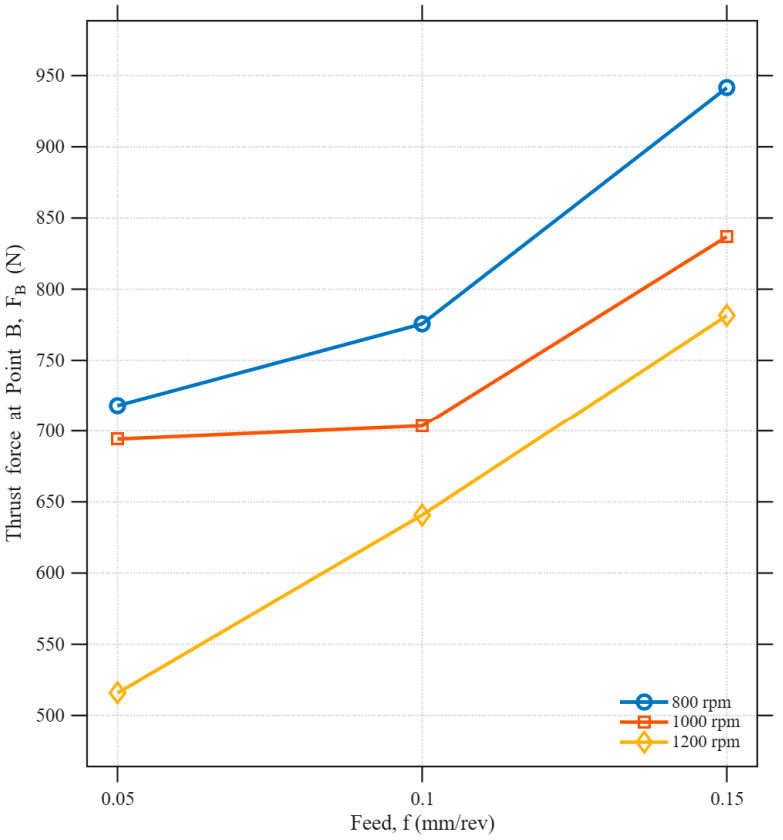

(**b**)

Figure 7. Effect of process parameters on thrust force for (**a**) Point A and (**b**) Point B.

3.2. Effect of Cutting Parameters on Residual Stress

Both hoop and axial residual stresses were measured in this study, as shown in Tables 5 and 6. However, drilling imposes its primary load through the axial thrust force, which governs subsurface deformation. Because no circumferential cutting load exists during drilling, hoop stress arises only as a secondary outcome of chip flow, side-wall friction and local thermal gradients. It is therefore not a sensitive or physically dominant indicator of drilling-induced energy input. For this reason, the residual stress analysis focuses exclusively on axial stress, which directly reflects the primary deformation mechanics of drilling.

The interpretation of the ANOVA results in this study must consider the limitations of the experimental design. The full factorial layout with nine tests and a single measurement for each cutting condition results in a low number of residual degrees of freedom. This reduces the statistical sensitivity of the F-test and makes it more difficult to detect significant differences among factors. In addition, drilling-induced residual stresses, especially at the exit side, are known to exhibit high variability because of breakout related deformation and the sensitivity of X-ray diffraction measurements to local microstructural differences. These conditions explain why several factors did not reach statistical significance even though clear mechanical trends are present in the measured data. For this reason, the ANOVA findings in this work should be considered as supportive trends rather than strong statistical proof. A more detailed statistical evaluation would require repeated tests and a larger set of measurement locations.

Due to the statistically insignificant ANOVA results ($p > 0.05$ for both feed and spindle speed), the axial stress values reported in Table 8a,b were not included in a detailed statistical evaluation. The lack of significance is mainly attributed to the limited number of experiments (n = 9), the high inherent variability of residual stress measurements, and the complex subsurface deformation mechanisms that occur during drilling. Despite this statistical limitation, the measured axial stress data still provide meaningful mechanical insight into how drilling parameters influence residual stress formation.

Table 8. (**a**) Two-way ANOVA results for axial residual stress at Point A with feed per revolution (f) and spindle speed (n) as factors. (**b**) Two-way ANOVA results for axial residual stress at Point B with feed per revolution (f) and spindle speed (n) as factors.

(**a**)					
Source	**Analysis of Variance**				
	DF	**Adj SS**	**Adj MS**	**F Value**	***p* Value**
Feed Per Rev. (mm/rev)	2	1610.93	805.46	0.934	0.4647
n (rpm)	2	2002.02	1001.01	1.161	0.4004
Error	4	3449.39	862.35	-	-
Total	8	7062.34	-	-	-
(**b**)					
Source	**Analysis of Variance**				
	DF	**Adj SS**	**Adj MS**	**F Value**	***p* Value**
Feed Per Rev. (mm/rev)	2	5859.98	2929.99	2.478	0.1995
n (rpm)	2	8958.38	4479.19	3.789	0.1195
Error	4	4729.12	1182.28	-	-
Total	8	19,547.48	-	-	-

The interpretation of the residual stress results must also consider the measurement related uncertainty of the X-ray diffraction method. The XRD values obtained in this study showed standard deviations that were generally acceptable at the entrance side but noticeably higher at the exit side. This behavior is expected because breakthrough causes local variations in plastic deformation, irregular chip separation, and micro geometry changes along the cut surface. These factors lead to peak broadening and a reduction in the linearity of the sin squared psi fit, which increases the spread of the calculated stress values. Therefore, the higher standard deviations observed at Point B do not indicate an experimental error but rather reflect the inherent instability of the drilling exit zone and the sensitivity of the XRD technique to local microstructural variations. These measurement effects should be taken into account when comparing stress magnitudes across different drilling conditions.

The axial residual stresses exhibit clear physical trends that are consistent with the mechanics of drilling. Across all cutting conditions, increasing the feed per revolution resulted in more compressive axial stresses at both measurement points. This behavior is directly related to the increase in thrust force, which acts purely in the axial direction and is the primary driver of subsurface plastic deformation during drilling. Higher feed rates increase chip load, enlarge the plastic shear zone, and intensify the compressive axial stress field beneath the drill tip. Similar relationships between feed rate, thrust force, and compressive residual stress have been reported in experimental investigations of residual stresses induced by drilling [28,29].

Spindle speed demonstrated the opposite trend, where increasing the cutting speed generally reduced the magnitude of compressive axial stress. This reduction can be attributed to thermally assisted softening of the workpiece material at elevated temperatures, which decreases resistance to plastic deformation and limits the accumulation of compressive stresses. In addition, higher spindle speeds improve chip evacuation and reduce tool–workpiece friction, thereby weakening the thermo-mechanical coupling responsible for subsurface stress buildup. Comparable thermal history-driven stress relaxation mechanisms during drilling have been reported in the literature [13].

A consistent asymmetry was observed between the two measurement locations. Axial stresses at Point B (exit side) were generally more compressive than those at Point A (entrance side), reflecting the well-known breakthrough mechanics of drilling. At the exit side, chip flow becomes more unstable and material support decreases, which intensifies thrust force fluctuations and enhances plastic strain just before breakout. This phenomenon is well documented in hole-making literature and has been associated with increased exit-side residual stresses and surface integrity degradation during drilling [27–29]. Overall, although the axial stress values did not show statistically significant differences in the ANOVA test, the mechanical trends observed in Table 8a,b are consistent, physically meaningful, and in agreement with previously reported findings in the literature. Feed per revolution remains the dominant factor influencing axial stress formation, while spindle speed primarily affects the thermal and frictional environment that governs stress relaxation. The exit-side measurements confirm that breakthrough deformation is a critical stage in the development of drilling-induced residual stresses.

3.3. Effect of Active Work on Residual Stress

In machining, one of the most decisive parameters governing subsurface residual stress formation is the total thermo-mechanical energy delivered into the cutting zone, expressed as active work (W_a). Previous machining studies have shown that increased mechanical energy input enlarges the plastic deformation zone and intensifies thermal accumulation, both of which directly influence the resulting residual stress state [8,9]. In

the present study, the relationship between active work and axial residual stress generated during drilling is illustrated in Figures 8 and 9.

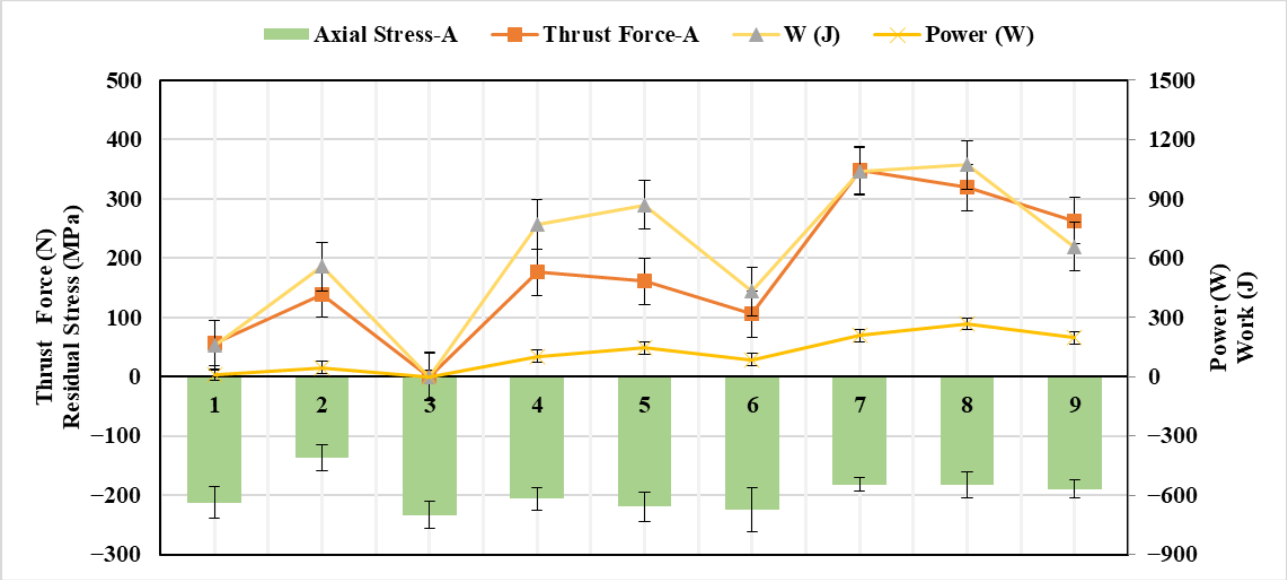

Figure 8. The effects of thrust force, power, and active work on the residual stress in the drilling operation of 7075-T6 for Axial direction in Point A.

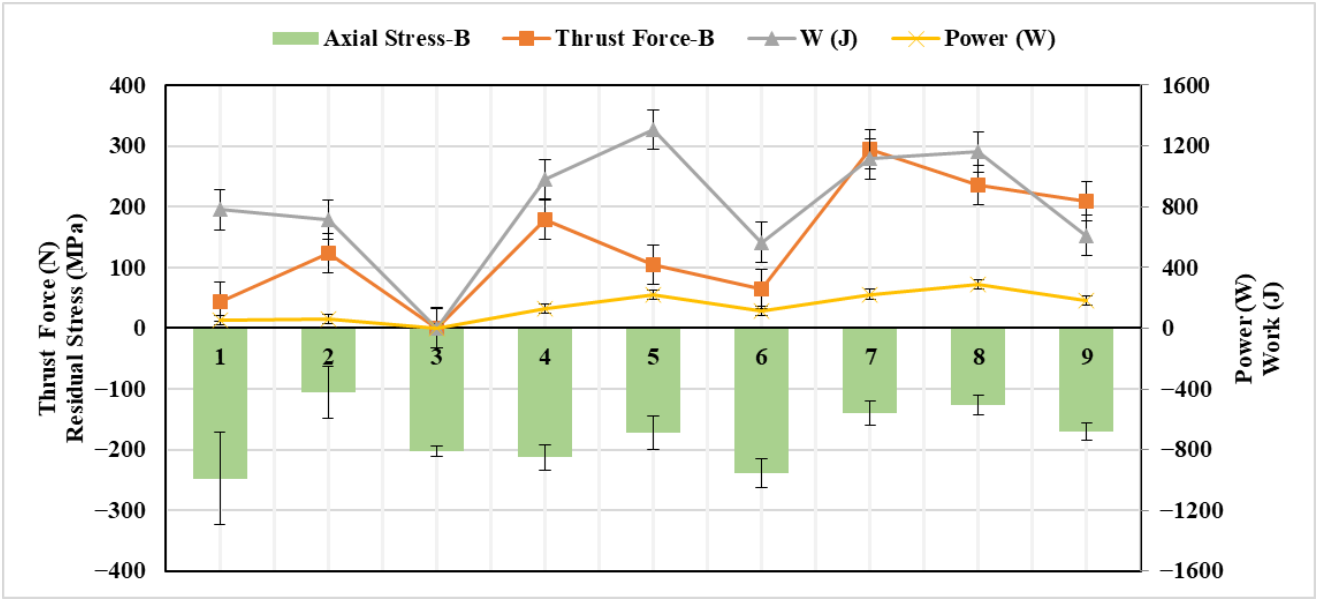

Figure 9. The effects of thrust force, power, and active work on the residual stress in the drilling operation of 7075-T6 for Axial direction in Point B.

Across all nine drilling experiments, the cutting parameters produced a systematic and predictable influence on active work. A closer examination of the data reveals a clear relationship between active work and axial residual stress at both measurement locations.

At Point A, lower energy input generally produces more stable and higher compressive stress levels. As the active work increased, a gradual reduction in the magnitude of compressive axial stress was observed. This behavior reflects a mechanically dominated deformation regime in which increasing plastic deformation progressively relaxes compressive stresses.

The behavior at Point B follows a similar trend but with a much stronger sensitivity to energy input. With increasing active work, the reduction in compressive axial stress became more pronounced at the exit side. This behavior can be attributed to the combined influence of thermal softening and deformation instability during drill breakthrough, where loss of material support and localized heat accumulation promote stress relaxation [9,13].

Feed per revolution was identified as the dominant factor influencing active work, since increasing feed substantially elevated thrust force and torque, leading to higher cutting power and total energy input. In contrast, spindle speed exhibited an inverse relationship with active work. Higher spindle speeds reduced friction, improved chip evacuation, and promoted thermally assisted softening, thereby lowering torque and overall energy demand. Similar trends have been reported in drilling and machining studies on aluminum alloys, where feed primarily governs mechanical energy input while cutting speed mainly affects the thermal and frictional conditions of the process [9,23].

Point A corresponds to a stable cutting region where the drill is fully supported by the material and deformation is predominantly mechanical. Consequently, residual stress evolution at this location follows a relatively smooth, mechanically controlled response to increasing active work. Point B, in contrast, represents the most unstable stage of drilling. Breakthrough is characterized by loss of material support, irregular chip formation, and localized heat concentration, causing residual stress formation to be governed primarily by thermal effects. The stronger stress relaxation observed at the exit side confirms that breakthrough deformation is a critical stage in drilling-induced residual stress development [19,23].

Although a fully quantitative formulation of the relationship between active work and residual stress would require direct temperature measurements and advanced thermo-mechanical modelling, the qualitative trends observed in Figures 8 and 9 can be consistently interpreted based on established drilling mechanics. Active work represents the cumulative thermo-mechanical energy delivered into the cutting zone and therefore governs both subsurface plastic deformation and heat accumulation during drilling. As the active work increases, the balance between mechanically-induced compressive stresses and thermally driven stress relaxation progressively shifts, resulting in a reduction in the magnitude of compressive axial residual stress. This behavior indicates that residual stress formation during drilling is controlled by the combined contribution of mechanical loading and thermal exposure rather than by a single process parameter.

The difference in sensitivity observed between Point A and Point B further supports this interpretation. At Point A, where the drill is fully supported by the surrounding material, residual stress evolution is predominantly governed by mechanically driven plastic deformation, leading to a relatively gradual response to increasing active work. In contrast, Point B corresponds to the breakthrough stage of drilling, where loss of material support, unstable chip formation, and localized heat concentration intensify thermo-mechanical effects. Under these conditions, increases in active work promote more pronounced stress relaxation, explaining the stronger qualitative correlation observed at the hole exit. These observations demonstrate that active work serves as a physically meaningful indicator for interpreting drilling-induced residual stress evolution, even when the analysis is limited to qualitative trends.

Finally, the behavior observed in this drilling study is in strong agreement with the mechanism reported by Tok et al. [8], where increasing cutting energy during turning of hot-forged AA7075 led to a transition from high compressive stress levels toward reduced compressive or tensile states. This parallel confirms that both drilling and turning of AA7075-T6 are governed by a unified energy-controlled thermo-mechanical balance and

demonstrates that active work is a robust predictor of residual stress evolution across multiple machining processes.

4. Conclusions

This study investigated the influence of drilling parameters on residual stress formation in hot-forged and T6-heat-treated AA7075. Based on force, torque, power, active work, and XRD measurements collected at two critical locations along the hole (Point A: entrance, Point B: exit), the following conclusions can be drawn:

- Feed rate was identified as the dominant parameter controlling drilling mechanics. Increasing feed significantly elevated thrust force, torque, cutting power, and active work, leading to deeper plastic deformation and higher compressive residual stresses. Conversely, higher spindle speeds reduced mechanical loads due to improved chip evacuation and thermally assisted softening.
- Residual stresses exhibited clear directional and positional asymmetry. Exit-side (Point B) stresses were more compressive due to breakthrough effects, reflecting unstable deformation, chip thickening, and restricted chip flow during drill breakthrough.
- Active work played a decisive role in governing residual stress evolution. For both measurement locations, active work was inversely related to compressive stress. At Point A, the reduction was dominated by mechanically driven plastic strain, whereas at Point B, thermally driven softening and breakout-induced instability produced a faster relaxation of compressive stresses.
- The results confirm that residual stress formation in drilling is controlled by the interaction between thermal and mechanical effects, consistent with behavior observed in other machining processes. Mechanical effects tended to promote compressive stresses, while thermal effects shifted the stress state toward tensile values.
- The transition between mechanical-dominated and thermal-dominated regimes was clearly observed. Under low-energy conditions, compressive stresses persisted due to mechanically dominated deformation. Under high-energy conditions, particularly near the hole exit, localized heat accumulation and breakthrough instability markedly reduced compressive stresses, illustrating the same thermal mechanical competition widely reported in machining literature.
- The observed behavior aligns with previously reported findings on machining of AA7075. The similarity between drilling and turning indicates that residual stress generation in AA7075-T6 is driven by a unified, energy-controlled thermo-mechanical mechanism. Accordingly, active work serves as a robust and generalizable predictor for understanding and optimizing residual stress development across multi-stage machining operations.

Overall, the results highlight the critical importance of controlling feed rate, spindle speed, and drilling energy input to achieve desirable residual stress states and improved surface integrity in high-strength aluminum components. These findings enhance the understanding of machining-induced stresses in precipitation-hardened alloys and support the development of predictive, energy-based residual stress models for advanced manufacturing applications.

Despite the insights provided by the present study, several limitations should be acknowledged. First, the investigation was conducted within a limited range of cutting parameters, focusing on three spindle speeds and three feed rates under dry drilling conditions. Second, due to the high cost associated with X-ray diffraction (XRD) measurements, residual stresses were measured only once for each drilling condition, and the analysis was restricted to near-surface stresses at two specific locations along the hole depth. In addition, XRD measurements inherently involve uncertainties related to surface sensitivity, elastic

constants, and local microstructural variations. Furthermore, complementary analyses such as chip morphology, tool wear evolution, and direct temperature measurements were not included in the present work.

Future studies will therefore focus on expanding the cutting parameter space, increasing experimental repeatability, and integrating temperature measurements together with chip morphology and tool wear characterization. Such combined thermo-mechanical analyses are expected to provide a more comprehensive understanding of residual stress formation mechanisms and to further improve the predictive capability of energy-based indicators for drilling-induced residual stresses.

Author Contributions: Conceptualization, G.T. and M.B.; methodology, G.T.; software, G.T.; validation, G.T., A.T.D. and A.T.K.; formal analysis, G.T.; investigation, G.T.; resources, M.B.; data curation, G.T.; writing—original draft preparation, G.T.; writing—review and editing, G.T., M.B. and A.T.K.; visualization, G.T.; supervision, M.B. and A.T.K.; project administration, M.B. All authors have read and agreed to the published version of the manuscript.

Funding: This research received no external funding. The APC was funded by the authors.

Data Availability Statement: Not applicable.

Acknowledgments: The authors would like to thank the Birinci Otomotiv A.Ş for equipment and facility support and Simultura Material Technologies Inc. for residual stress measurements.

Conflicts of Interest: The authors declare no conflicts of interest.

References

1. Aurrekoetxea, M.; López de Lacalle, L.N.; Zelaieta, O.; Llanos, I. In-Process Machining Distortion Prediction Method Based on Bulk Residual Stresses Estimation from Reduced Layer Removal. *J. Manuf. Mater. Process.* **2024**, *8*, 9. [CrossRef]
2. Storchak, M.; Stehle, T.; Möhring, H.-C. Numerical Modeling of Cutting Characteristics during Short Hole Drilling: Part 2—Modeling of Thermal Characteristics. *J. Manuf. Mater. Process.* **2024**, *8*, 13. [CrossRef]
3. Mondelin, A.; Valiorgue, F.; Rech, J.; Coret, M. 3D Hybrid Numerical Model of Residual Stresses: Numerical—Sensitivity to Cutting Parameters When Turning 15-5PH Stainless Steel. *J. Manuf. Mater. Process.* **2021**, *5*, 70. [CrossRef]
4. Denkena, B.; Grove, T.; Maier, H.J. Analysis of the influence of mechanical loads on residual stresses in cutting processes. *CIRP Ann.* **2011**, *60*, 121–124.
5. Luo, H.; Fu, J.; Wu, T.; Chen, N.; Li, H. Numerical simulation and experimental study on the drilling process of 7075-T6 aerospace aluminum alloy. *Materials* **2021**, *14*, 553. [CrossRef]
6. Kara, M.E.; Kuzu, A.T.; Bakkal, M. The development of a hybrid cutting model for workpiece temperature distribution via advection heat partition approach. *Int. J. Adv. Manuf. Technol.* **2023**, *126*, 4283–4295. [CrossRef]
7. Tok, G.; Dincer, A.T.; Kuzu, A.T.; Bakkal, M. Predictive modelling of surface roughness and residual stress induced by milling of hot-forged and heat-treated AA7075. *Int. J. Adv. Manuf. Technol.* **2025**, *141*, 5793–5806. [CrossRef]
8. Tok, G.; Kuzu, A.T.; Bakkal, M. Investigation of residual stresses induced by turning of hot-forged and heat-treated AA7075. *Int. J. Adv. Manuf. Technol.* **2024**, *135*, 4823–4836. [CrossRef]
9. Biermann, D.; Heilmann, M.; Kirschner, M. Thermal aspects in deep hole drilling of aluminium. *Procedia CIRP* **2012**, *3*, 185–190. [CrossRef]
10. Tai, B.L.; Stephenson, D.A.; Shih, A.J. An inverse heat transfer method for determining workpiece temperature in minimum quantity lubrication deep hole drilling. *J. Manuf. Sci. Eng.* **2003**, *125*, 613–620. [CrossRef]
11. Li, S.; Zhang, D.; Liu, C.; Tang, H. Exit burr height mechanistic modeling and experimental validation for low-frequency vibration assisted drilling of aluminum 7075-T6 alloy. *J. Manuf. Process.* **2020**, *56*, 350–361. [CrossRef]
12. Le Coz, G.; Marinescu, M.; Devillez, A.; Dudzinski, D.; Velnom, L. Measuring temperature of rotating cutting tools: Application to MQL drilling and dry milling of aerospace alloys. *Appl. Therm. Eng.* **2012**, *36*, 434–441. [CrossRef]
13. Chenegrin, K.; Bouscaud, D.; Girinon, M.; Karaouni, H.; Bergheau, J.-M.; Feulvarch, E. Study of the thermal history upon residual stresses during the dry drilling of Inconel 718. *Metals* **2022**, *12*, 305. [CrossRef]
14. *EN ISO 6506-1*; Metallic Materials—Brinell Hardness Test—Part 1: Test Method. International Organization for Standardization (ISO): Geneva, Switzerland, 2014.
15. *EN ISO 6892-1*; Metallic Materials—Tensile Testing—Part 1: Method of Test at Room Temperature. International Organization for Standardization (ISO): Geneva, Switzerland, 2019.

16. *EN 573-3*; Aluminium and Aluminium Alloys—Chemical Composition and Form of Wrought Products—Part 3: Chemical Composition and Form of Products. European Committee for Standardization (CEN): Brussels, Belgium, 2019.
17. *EN 15305*; Non-Destructive Testing—Test Method for Residual Stress Analysis by X-Ray Diffraction. European Committee for Standardization (CEN): Brussels, Belgium, 2008.
18. Fitzpatrick, M.E.; Fry, A.T.; Holdway, P.; Kandil, F.A.; Shackleton, J.; Suominen, L. *Determination of Residual Stresses by X-Ray Diffraction*; Good Practice Guide No. 52, Issue 2; National Physical Laboratory (NPL): Teddington, UK, 2005.
19. Kwong, J.; Axinte, D.A.; Withers, P.J. The sensitivity of Ni-based superalloy to hole making operations: Influence of process parameters on subsurface damage and residual stress. *J. Mater. Process. Technol.* **2009**, *209*, 3968–3977. [CrossRef]
20. Tai, L.-J. Thermal Modeling of Workpiece Temperature and Distortion in MQL Deep-Hole Drilling. Ph.D. Thesis, University of Michigan, Ann Arbor, MI, USA, 2011.
21. Choe, J.-H.; Ha, J.H.; Kim, J.; Kim, D.M. Surface characteristics and residual stress variation in semi-deep hole machining of Ti6Al4V ELI with low-frequency vibration-assisted drilling. *J. Manuf. Mater. Process.* **2023**, *7*, 209. [CrossRef]
22. Parasuraman, S.; Elamvazuthi, I.; Kanagaraj, G.; Natarajan, E.; Pugazhenthi, A. Assessments of Process Parameters on Cutting Force and Surface Roughness during Drilling of AA7075/TiB_2 In Situ Composite. *Materials* **2021**, *14*, 1726. [CrossRef]
23. Gökçe, H.; Bibercı, M.A. Investigation of thrust force, drill bit temperature and burr height in the drilling of aluminum alloy used in ammunition wing drive systems. *Exp. Tech.* **2022**, *46*, 691–705. [CrossRef]
24. Akdulum, A.; Kayir, Y. Experimental investigation and optimization of process stability in drilling of Al 7075-T651 using indexable insert drills. *J. Braz. Soc. Mech. Sci. Eng.* **2023**, *45*, 429. [CrossRef]
25. Patil, A.; Hebasur, V.I.; Mahale, R.; Tambrallimath, V.; Divya, G.S.; Nagraj, B.; Kattimani, P.C. Quantitative analysis of frictional forces and their impact on drilling efficiency in aluminum alloy machining. *J. Inst. Eng. India Ser. C* **2024**, *105*, 5. [CrossRef]
26. Sikander, A.; Ullah, B.; Naseem, M.S.; Channar, H.R.; Aslam, M. Analysis of dry and cryogenic drilling on hole quality in AA2024-T6 using HSS and HSS-Co tools. *J. King Saud. Univ.—Eng. Sci.* **2025**, *37*, 15. [CrossRef]
27. Chao, Y.; Ren, C.; Zhang, D. Development of a predictive analytical cutting force and torque model for flat-bottom drilling of metals using a mechanistic approach. *J. Manuf. Process.* **2020**, *27*, 1–25.
28. Girinon, M.; Valiorgue, F.; Rech, J.; Feulvarch, E. Development of a procedure to characterize residual stresses induced by drilling. *Procedia CIRP* **2016**, *45*, 79–82. [CrossRef]
29. Nobre, J.P.; Outeiro, J.C. Evaluating residual stresses induced by drilling using an experimental–numerical methodology. *Procedia CIRP* **2015**, *31*, 215–220. [CrossRef]